Engineering and Technology Journal
Journal homepage: https://etj.uotechnology.edu.iq

Effect of nano and nanocomposite coating on pool boiling heat transfer

Ali M. H. Al-Obaidy*, Ekhlas M. Fayyadh, Amer M. Al-Dabagh
Mechanical Engineering Dept., University of Technology-Iraq, Alsina'a street, 10066 Baghdad, Iraq.
*Corresponding author Email: me.19.29@grad.uotechnology.edu.iq

HIGHLIGHTS

- Four surfaces made of copper were used in this study: smooth, CNT (1 g), GNPs (1 g), and (CNT-GNPs (1:1) g).
- The maximum HTC is obtained by (CNT-GNPs (1:1) g) surface with 154%.
- The mixed wettability of nanocomposite coating can enhance the heat transfer coefficient (HTC).

ARTICLE INFO

Handling editor: Mohammed A. Fayad

Keywords:
Pool boiling; Coating; GNPs; CNT; Nanocomposite coating; Nanocoating; Four steps electrodeposition; Hydrophilic; Hydrophobic.

ABSTRACT

High heat generation is the main problem that sophisticated electronic devices can suffer. The pool boiling process can offer an excellent heat dispassion at constant temperatures. Therefore, it is one of the most powerful cooling processes used in nuclear power plants, data centers, air conditioning, etc. Because of that, enhancing pool boiling has become a goal of many recent investigations. The current paper presents an experimental study to evaluate the effect of nano and nanocomposite coating on the performance of pool boiling of deionized water under atmospheric pressure. Four surfaces made of copper were used in this study: smooth, CNT (1 g), GNPs (1 g), and (CNT-GNPs (1:1) g) surfaces. A four-step electro-deposition method was used to fabricate a nickel coating using the abovementioned materials. The variation in coating materials offers different surface wettability and roughness to the fabricated surfaces. The experiment's outcome revealed that the hydrophilic material can enhance the critical heat flux (CHF). The mixed wettability obtained by the nanocomposite coating can improve the heat transfer coefficient (HTC). Maximum enhancement in the CHF is obtained by GNPs (1 g) surface with 102%, while the maximum HTC is obtained by (CNT-GNPs (1:1) g) surface with 154% when it is compared with the plain surface.

1. Introduction

Recently, there has been a significant emphasis on two-phase heat transfer because of the increasing need for effective heat dissipation in high heat flux systems. Unlike non-phase change processes, pool boiling heat transfer is a reliable and efficient approach for high heat flow systems. It has been used in several technological fields, such as nuclear reactors, high-performance electronics, power plants, and spacecraft [1-14]. Increasing the surface roughness, wettability, porosity, etc, may further enhance the total heat transfer efficiency. The deposition of nanocoating on a heating surface has attracted considerable attention recently because to its proven effectiveness in increasing both the heat transfer coefficient (HTC) and the critical heat flux (CHF) [15]. Researchers have attempted to modify the surface coating on a plain surface to improve the efficiency of pool boiling.

The effect of coating on heat transfer during pool boiling has been the subject of numerous studies. The electro-deposition coating technique is one of the most simple and cheap methods available. Also, the electro-deposition method can control the pore size and coating layer thickness. Therefore, Patil et al. [16] obtained a maximum HTC (176 kW/m^2.K) by microstructures resembling cauliflower that were produced using a lower current density than those resembling open dishes, which were produced using a greater current density. Modifying the electro-deposited porous surfaces is possible by swirling the electrolyte during the deposition process. Gupta and Misra [17] produced Cu-Al_2O_3 nanocomposite coatings and applied them to Cu surfaces. They reported 260% and 68% improvement in HTC and CHF, respectively, compared to the bare Cu surface. In another experiment [4], the same team of researchers created Cu-TiO_2 composite coatings on copper surfaces. Compared to a bare Cu surface, the results showed that the HTC and CHF of surfaces coated with a Cu-TiO_2 composite were 185% and 86%, respectively. Li et al. [18] produced three-tier hierarchical nano-engineered surfaces by stirring the electrolyte throughout the electro-deposition process.

Micro-pores on the first layer, dendritic structures on the second layer, and Cu nanoparticles on the third layer were found to increase the density of nucleation sites, direct the course of bubble evolution, and boost the wicking ability in that order. The maximum CHF of the third-level hierarchical surface was also rather high, coming in at roughly (400 W/cm^2), equivalent to an

http://doi.org/10.30684/etj.2024.149236.1742
Received 02 May 2024; Received in revised form 01 June 2024; Accepted 07 June 2024; Available online 10 July 2024
2412-0758/University of Technology-Iraq, Baghdad, Iraq

increase of around (245%). Rishi et al. [19] also used the two steps of electro-deposition to create graphene nano-platelets (GNPs)-Cu porous coating. The ultra hydrophilic (GNPs)-Cu coatings can increase the CHF and the HTC by 130% and 290%, respectively. Mo et al. [17] used the electro-deposition method to create a porous honeycomb surface. The results of the pool boiling experiments indicate that a surface with a radial diameter gradient can enhance the water replenishment process and improve re-wetting. Consequently, such a surface's heat transfer coefficient (HTC) can reach values 1.4 to 1.5 times higher than those observed for surfaces with a uniform pore diameter. In their study, Katarkar et al. [18] utilize a two-step electro-deposition process, incorporating graphene nano-platelets (GNP) within the electrolyte solution. Four concentrations of 100, 200, 300, and 400 mg/L of GNPs were employed. Furthermore, it was observed that the surface porosity, thickness, and roughness increased when the concentration of GNPs in the electrolyte solution rose. The experiment results demonstrated that the HTC sample with a concentration of GNP at 400 mg/L exhibited a greater outcome of 173.8% than the plain sample.

Surface wettability has a significant impact on boiling heat transfer. A surface is wettable (i.e., hydrophilic) if the contact angle between a liquid and a solid substrate is less than 90 degrees, and hydrophobic if the contact angle is greater than 90 degrees. The diameter of departure bubble increases with contact angle increase. Numerous studies have been done in this area, and it has been shown that the surface's wettability significantly influences heat transfer during boiling. Yim et al. [19] studied the wettability effect on the pool boiling heat transfer over the TiO_2 nanomaterial deposited hydrophilic TiO_2 coated and the bared aluminum surface. The boiling heat transfer of the uncoated surface was performed in extreme comparison with the hydrophilic TiO_2 surface. Furthermore, an increase in the HTC for the TiO_2 deposited surface was (64%) in comparison with the uncoated surface. The boiling performance of Cr and FeCrAl-coated stainless steel substrates with the modulation of micro-/nano-scaled surface topography was studied by Son et al. [20]. All coated surfaces generated by the sputtering technique inherently consisted of fine nano-scale surface topographical structure. The surface features of the coatings showing both nano-scaled structure (controlled by sputter deposition parameters) and microscale structure (modulated by surface roughness of substrates) provided super hydrophilic characteristics, resulting in enhancement of the CHF and HTC values up to 34% and 24%, respectively on samples coated with FeCrAl surface, while they achieved an enhancement of CHF and HTC with 27% and 15%, respectively on samples coated with Cr, as compared with uncoated surface. Fan et al. [21] manifested that the TiO_2-covered Cund Ti surfaces resulted in a hydrophilic surface with enhancement of the CHF of 40% compared to a plain surface through the Novec 7100 dielectric fluid boiling. Also, the Ti substrate concealed via the TiO_2 nanotube array enhanced the HTC by (65%). In comparison, the copper substrate covered in nanotubes had an average HTC of 20% less than that of the uncoated copper surface.

In lower heat flux circumstances, the early commencement of boiling is caused by the reduced free energy demand for nucleation in hydrophobic surfaces. However, at higher heat fluxes, the sudden formation of bubbles across the surface results in lower heat transfer for hydrophobic surfaces compared to hydrophilic ones. Bourdon et al. [22] studied the pool boiling heat transfer upon the glass surface for the hydrophobic and hydrophilic wettability. And, for the hydrophobic case, the ONB was performed beyond the superheat temperature (3.5 °C) as well as the HTC that ranges from (1.5 kW/m^2K) to (4 kW/m^2K). In contrast, the HTC was maintained as the convection regime's component in the hydrophilic example despite a superheat of more than 37 °C and the presence of boiling. The researchers conducted the initial bubble appearance too early for the hydrophobic than the hydrophilic. Also, the reduction in the wettability provided an increase to a reduction in the ONB. However, researchers started to think about surfaces with hybrid wettability because surfaces with homogenous wettability offer benefits and limitations in heat transfer improvement. Lim et al. [23] manufactured biphilic surfaces by coating porous superhydrophobic materials on SiO_2/Si bare heaters. The largest enhancement in the HTC was up to 35% in some biophilic surface coatings. The enhancement on the biophilic surfaces was attributed to the augmentation of nucleation sites due to the differences in the wetting state and thermal conductivity between the hydrophilic and hydrophobic regions. Surface wettability has recently been found to be crucial in controlling interfacial heat transfer. For instance, Li et al. [24] examined the variation effect of the hydrophilic/hydrophobic area ratio of the copper surface on the bubble nucleation, growth, departure, and heat transfer. Four surfaces were fabricated with different hydrophilic/hydrophobic area ratios. Results showed that the associated heat transfer performance is directly related to the ratio of the hydrophilic surface area to the hydrophobic one. The CHF of the 5:1 mixed surface increased by 26% compared to a pure hydrophobic surface, whereas the CHF of the 1:1 mixed surface increased by 16%. Park et al. [25] analyzed the amalgamation of electrospray and the chemical bath deposition methods for reaching a hierarchical structure of the ZnO nanowires alongside the Cu surface. It was found that the optimal combination of a bare hydrophobic surface and a hydrophilic surface covered with ZnO nanowires yielded the highest CHF and HTC. Moreover, the utilization of ZnO nanowires augmented the buoyancy force, enhancing the CHF till (40%) compared with the non-coated specimen.

The review elucidated that porosity, wettability, and surface roughness can be achieved by coating surfaces. Many techniques have been employed to create microporous coatings on the heating surface. These techniques caused the enhancement of boiling heat transfer coefficient and CHF within the range of (36-300%) and (33-350%), respectively, compared to a plain surface. It depended upon the coating material and coating methods. However, when the wettability of the coating surface is hydrophobic, it induces the boiling onset at the wall's lower degrees of superheat owing to the positive vapor trapping. It is more efficient and appreciably increases the boiling characteristics. Still, the durability of these surfaces with repeated trial runs will impact the lifetime and performance of the appliances, where the deformation of these surfaces was observed at higher heat flux during the pool boiling experiments. In other words, the ONB at low wall superheat temperature without departure of bubbles causes an increase in HTC at low heat flux. In contrast, the hydrophilic of coating surfaces has improved the re-wetting conduct and late critical heat flux. This gives ahigh HTC at high heat flux. However, the researchers start to investigate the impact of using surfaces with a hybrid wettability (hydrophilic-hydrophobic) on performance of pool boiling since the surfaces with a hybrid or mixed wettability have both effects of hydrophobic and hydphilic surfaces which can enhance the HTC in both regions of low and high heat flux. Therefore, This paper investigated the effect of nano- and nanocomposite coating on the performance of pool boiling using deionized water under atmospheric pressure, which offers the three kinds of wettability mentioned before. For this

purpose, four copper surfaces were used: smooth, two nanoparticle coatings with different materials, and one nanocomposite coating.

2. Experimental work

2.1 Experimental rig

The pool boiling setup, shown in Figure 1, was used to conduct the experiments in the present study. The setup includes a boiling chamber, heating components, a condenser unit, data acquisition hardware, and a power supply unit. The boiling chamber is cylindrical and made of stainless steel, with a height of 350 mm and an inner diameter of 120 mm. Two sight glass windows have been included within the boiling chamber to provide a visual observation. The boiling chamber was sealed by two cylindrical flanges, one at the top and one at the bottom. Four connecting rods and O-rings were used on each side to prevent any possible leak in the system. The top flange is made of aluminum. The apparatus had an aperture for the distilled water inlet, a thermocouple probe type K (T_1) for measuring bulk temperature, and inlet and outlet connections for the copper condenser. A copper tube wound in a coil functioned as a condenser for the system. The chiller unit maintains a consistent temperature in the condenser by supplying cooling water at the correct temperature and flow rate. The bottom flange was constructed from thermal Teflon and had two auxiliary heaters, each operating at 120 VDC and 200 W, controlled by Hayder to keep the bulk water temperature at saturation levels. The PID monitors the temperature of the liquid boiling chamber using a thermocouple (T_1). Furthermore, a 20 mm diameter center hole was created for inserting the heating element. The thermocouples were linked to a data logger device (Model AT4524-Applent Instruments Company) with an accuracy of ± 0.3 ºC, which was paired with a USB data logger (Model number ATN2 USBRS232) to collect temperature measurements.

2.2 Surface preparation

The plain copper test surfaces were made smooth by polishing. Hence, the used procedure can be summarized as follows: (1) The coarser surface roughness left over from the manufacturing process was removed by using 16 µm (600 grit) of emery papers with a circular motion for 30 seconds; (2) Primary polishing was conducted using 9 µm (1000 grit) of emery papers for 1 minute; (3) Additional polishing was accomplished using a grain size of 3 µm (1500 grit) and 0.1 µm (2500 grit) of the emery papers for two minutes, and (4) Removing any remaining residue and getting a smooth surface as a mirror was done by using Hippish Simi chrome polish with a delicate cotton pad. Finally, the copper test surface was washed with acetone and ethanol. Three surfaces were created using the electro-deposition coating method. Two of them were coated with nanoparticles: GNPs (1 g) and CNT (1 g). The last one was deposited with CNT-GNPs (1:1) g nanocomposite material. Mehdikhani et al. [26] outlined a four-step process followed by the electro-deposition technique. For the first 30 seconds, a current density of 109 mA/cm^2 (or 343 mA at 3.6 V) was applied, and for the second 1200 seconds, a current density of 36 mA/cm^2 (or 115 mA at 1.7 V) was applied. While steps three and four simply continue steps one and two. In addition, the needed thickness of the coating, 40 µm, dictates the current choice. An electrolyte solution containing 240 g/L of nickel sulfate ($NiSO_4.6H_2O$), 30 g/L of nickel chloride ($NiCl_2.6H_2O$), and 30-37.5 g/L of boric acid (H_3BO_3) was first made in a total volume of 250 mL. To evenly distribute the nanoparticles throughout the electrolyte solution, boric acid is used to adjust the pH before adding the solution to the specimens to be coated. The mixture is then stirred at 400 rpm for 60 minutes while the magnetic stirring is active. The coating method steps and the rotating stirring can keep constant thickness and homogeneous coating layers. All the surfaces were prepped for coating by being washed and polished using a solution of hydrochloric acid and ethanol ($HCL.5H_2O$ (1:1)). To remove any last traces of contamination from the copper surface, the substrate and the specimen were washed with distilled water. The copper substrate and its specimen are cathodes, whereas the nickel substrate is the anode in the electrolyte solution. The anode and cathode are 20 mm apart inside the coating electrolyte. Three surfaces were fabricated with three different materials: CNT (1 g), GNPs (1 g), and CNT-GNPs (1:1) g.

2.3 Procedure of experiment

During the degassing test, the transformer is connected to an electrical power source, and the power is turned on. The auxiliary heaters will be turned on full blast to bring the water temperature to saturation. So, when the water hits the saturation point, it is left to boil to get rid of any dissolved gases. That takes at least 45 minutes to finish. Since this is the case, testing in the experiment begins after the maximum point. A variable transformer, which needs power, can change the voltage going into the cartridge warmer from zero to higher voltages. The test section and working fluid had to be kept steady for about 15 minutes at each power source for the cartridge heater. Researchers used to think that a place was in a steady state when the temperature changed by about 0.1 ºC every two minutes [12]. After that, readings were made of the temperature, the voltage across the heater capsule, and current flow. Once the voltage across the cartridge heater was raised, the same steps were used to record data at the next heat input situation. These steps are carried out in a variety of heat flow conditions to get temperatures for a certain test area. The study only looked at heat flows between 0 and 3,400 kW/m^2 for safety reasons.

2.4 Surface characteristics measurements

In the current work, three surfaces were used: GNPs (1 g), CNT (1 g), and CNT-GNPs (1:1) g. Atomic Force Microscopy (AFM Naio Nanosurf Switzerland) was used to evaluate the surface roughness of four distinct boiling copper test surfaces. The average roughness of the surface under testing is the most important factor, which is defined as the arithmetic mean of the absolute values of the height of the surface profile from area scan data. Figure 2 is illustrated the AFM scanning images as follow: (a) Model-1 (smooth surface), (b) Model-2 (CNT 1g coated surface), (c) Model-3 (GNPs 1g coated surface), and (d) Model-4 (CNT-GNPs (1:1) g coated surface). The nucleate pool boiling heat transfer is significantly influenced by the surface wettability of the working liquid. The static contact angle is used as a metric for this. A sessile drop technique, which is applied

by the device model (CAMP110P – SIPLASMA), is used to determine the static contact angles of a surface by placing a tiny drop of water (micro milliliter) on it, and a camera takes the corresponding picture. Then, the tangents are sketched for the captured picture to determine the subsequent contact angle of the specimen. The contact angle measurements are illustrated in Figure 3 as follow: (a) Model-1 (smooth surface), (b) Model-2 (CNT 1g coated surface), (c) Model-3 (GNPs 1g coated surface), and (d) Model-4 (CNT-GNPs (1:1) g coated surface) . The porosity of the testing material was measured using Field Emission Scanning Microscopy (FE-SEM) in conjunction with Image-J software. The results of the analog image observed on the microscope are converted into digital images to be analyzed using Image-J. Porosity measurements are shown in Figure 4 as follow: (a) Model-2 (CNT 1g coated surface), (b) Model-3 (GNPs 1g coated surface), and (c) Model-4 (CNT-GNPs (1:1) g coated surface) The characteristics are listed in Table 1.

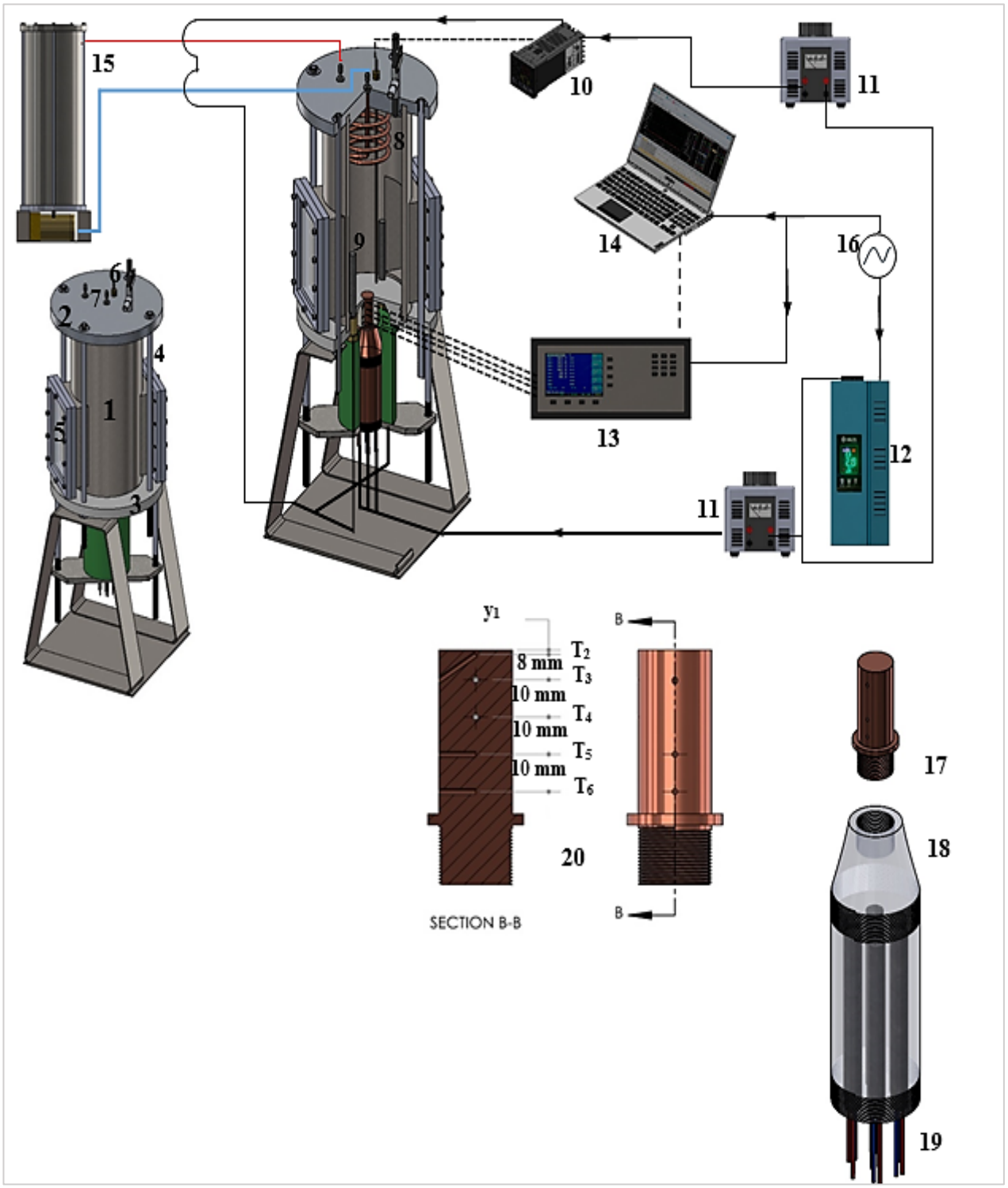

Figure 1: Experimental rig. 1. Boiling chamber vessel, 2. Upper flange, 3. Lower flange, 4. Connecting rod, 5. Sight glass, 6. Thermocouple probe, 7. Cooling water inlet and outlet, 8. Condenser coil, 9. Auxillary heater, 10. PID, 11. Variac, 12. Stabilizer, 13. Data logger, 14.PC, 15. Cooling tower, 16. Power source, 17. Heating surface block, 18. Copper block, 19. Main heaters 20. Heating surface block thermocouple distribution

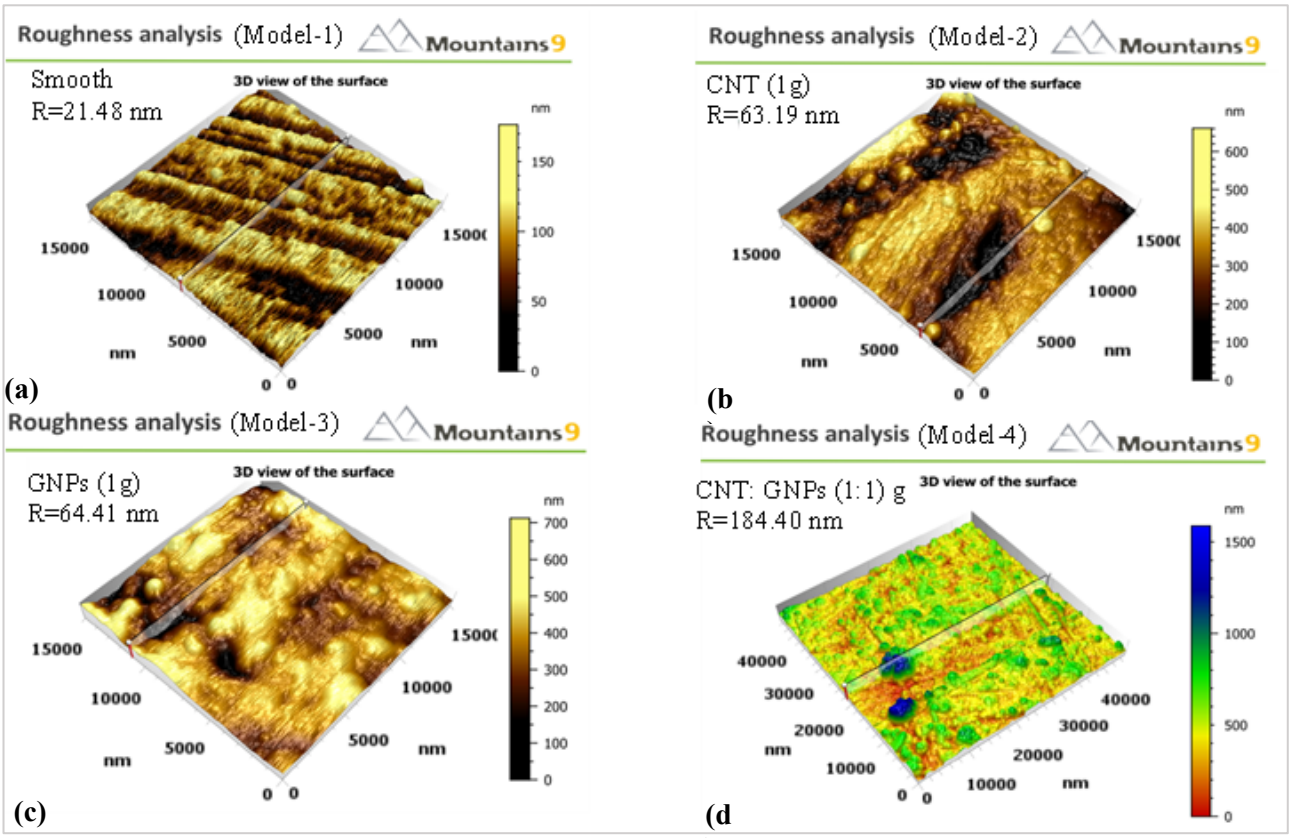

Figure 2: Roughness measurements of smooth and coated plain of copper test surfaces specimens by AFM (a) Model-1 (smooth surface) *R=21.48 nm*. (b) Model-2 (CNT 1g coated surface) *R=63.19 nm*. (c) Model-3 (GNPs 1g coated surface) *R=64.41 nm*. (d) Model-4 (CNT-GNPs (1:1) g coated surface) *R=184.4 nm*

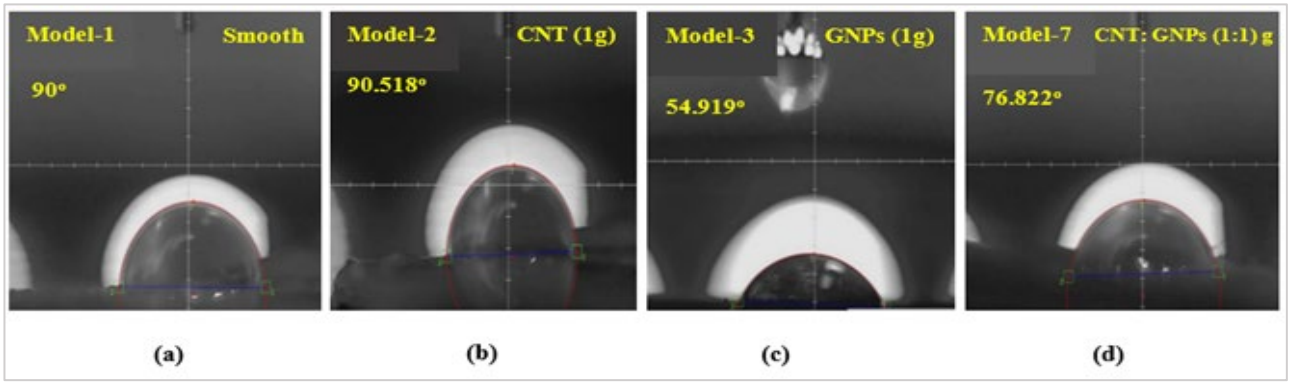

Figure 3: Contact angles for smooth and coated plain copper test surface specimens (a) Model-1 (smooth surface) $\theta=90^o$. (b) Model-2 (CNT 1g coated surface) $\theta=90.518^o$. (c) Model-3 (GNPs 1g coated surface) $\theta=54.919^o$. (d) Model-4 (CNT-GNPs (1:1) g coated surface) $\theta=76.822^o$

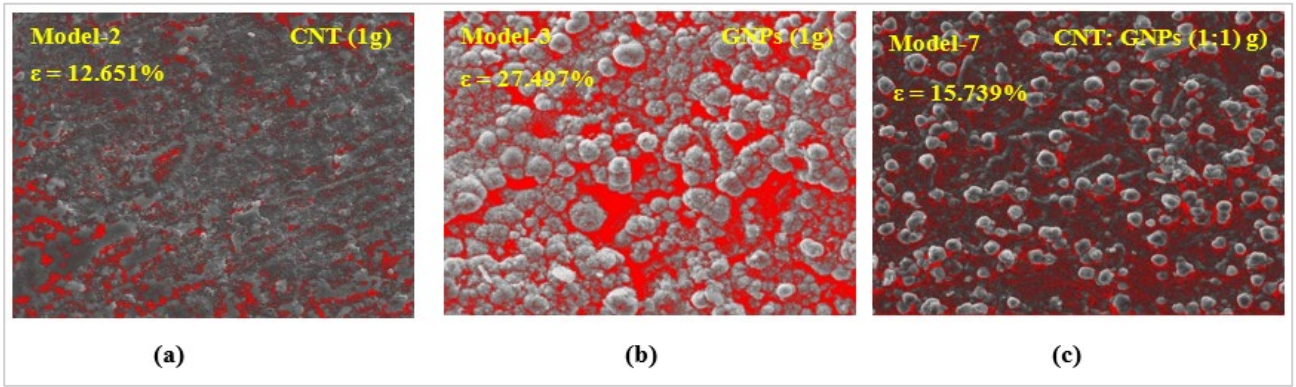

Figure 4: Porosity measurements of coated plain copper test surface specimens (a) Model-2 (CNT 1g coated surface) $\varepsilon=12.651\%$. (b) Model-3 (GNPs 1g coated surface) $\varepsilon=27.497\%$. (c) Model-4 (CNT-GNPs (1:1) g coated surface) $\varepsilon=15.739\%$

Table 1: Nano and nanocomposite-coated surface characteristics

Model	Contact angle (Degree)	Roughness (R)(nm)	Porosity (%)	Pore diameter (µm)	r, min (µm)	r, max (µm)
Model-1	90	0.02148	3.203	0.0003	0.006	181.8
Model-2	90.518	0.06319	12.651	0.1133	0.01	181.8
Model-3	54.919	0.06441	27.497	0.0005	0.007	148.78
Model-4	76.822	0.1844	15.739	0.0637	0.0091	177

3. Data reduction and uncertainties

The heat flux applied to the heat sink can be considered in one direction. The calculations, in this case, follow Fourier's law of heat transfer in the vertical direction [16,17] as below in Equation 1:

$$q = -k\frac{\mathrm{d}T}{\mathrm{d}y} \tag{1}$$

where k is the thermal conductivity of heating surface material (Copper). The temperature gradient is determined using backward Taylor's series approximation based on three points as expressed in Equation 2:

$$\frac{\mathrm{d}T}{\mathrm{d}y} = \frac{3T_3-4T_4+T_5}{2\Delta y} \tag{2}$$

Taylor's series is valid only with equal-spaced points. So, point 2 is not included in the above equation. The heat transfer coefficient can be evaluated using Equation 3 the Newton's law of heat transfer:

$$h = \frac{q}{T_s-T_l} \tag{3}$$

where T_l is the saturated temperature of the boiled liquid, and T_s is the heating surface temperature, which can be evaluated by Fourier's law also [30,31] as expressed in Equation 4:

$$T_s = T_2 - q\frac{y_1}{k} \tag{4}$$

T_2, T_3, T_4 and T_5 are points of thermocouples on the heat sink, as shown in Figure 1. y_1 is the space between the point of thermocouple 1 and the heating surface.

The heating group is made of more than one piece, which causes a lot of heat losses due to the gaps and thermal grease, whose thermal conductivity is far from that of copper. First, the provided heat flux must be calculated by the Equation 5 below:

$$q = \frac{VI}{A} \tag{5}$$

Then, Equation 1 will be subtracted from Equation 5 to obtain the losses.

The uncertainty is derived using Coleman et al. [30]. Therefore, the uncertainty of heat flux can be given by Equation 6 below:

$$U_{q"} = q"\left[\left(\frac{U_k}{k}\right)^2 + \left(\frac{U_{T_2}}{3T_2-4T_3+T_4}\right)^2 + \left(\frac{U_{T_3}}{3T_2-4T_3+T_4}\right)^2 + \left(\frac{U_{T_4}}{3T_2-4T_3+T_4}\right)^2 + \left(\frac{U_{\Delta y}}{\Delta y}\right)^2\right]^{0.5} \tag{6}$$

The uncertainty of surface temperature can be given by Equation 7:

$$U_{T_s} = (T_1 - T_s)\left[\left(\frac{U_{T_1}}{T_1-T_s}\right)^2 + \left(\frac{U_{q"}}{q"}\right)^2 + \left(\frac{U_{y_1}}{y_1}\right)^2 + \left(\frac{U_k}{k}\right)^2\right]^{0.5} \tag{7}$$

where $U_{q"}$, U_k, U_{T_1}, U_{T_2}, U_{T_3}, U_{T_4}, $U_{\Delta y}$, U_{T_s}, is the uncertainties of heat flux, thermal conductivity, thermocouples (2, 3, 4, and 5), length and surface temperature, respectively. All thermocouples were calibrated and found to be ±0.1 K. The greatest uncertainties in the heat flux and surface temperature readings were ±0.43% kW/m^2 and ±6%.

4. Results and Discussion

4.1 Experiments validation

To ensure that the measurement instruments and experimental setup were accurate, pool boiling curves were executed. Experimental data and known correlations from prior research were compared with the results from the smooth plain copper surface [33-36]. The comparison with the published data was evaluated using the mean absolute error (MAE) in the following manner which is given by Equation (8):

$$MAE = \frac{1}{n}\sum_{i=1}^{n}\frac{x_{pred,i}-x_{exp,i}}{x_{exp,i}} \times 100\% \quad (8)$$

where: x is the heat flux in this work, and n is the total number of data points.

The comparison can be shown in Figure 5. The present study gives a good agreement with the experimental data from Dharmendra et al. [31] and Wang et al. [34], with an MAE value of 8.28% and 13.63%, respectively. In addition, the current experimental results were compared to established correlations such as Jung et al. [33], and Cooper [34]. Figure 5 shows that the correlations for Jung et al. [33] and Cooper [34] give a good prediction with an MAE of 22.97% and 26.01%, respectively.

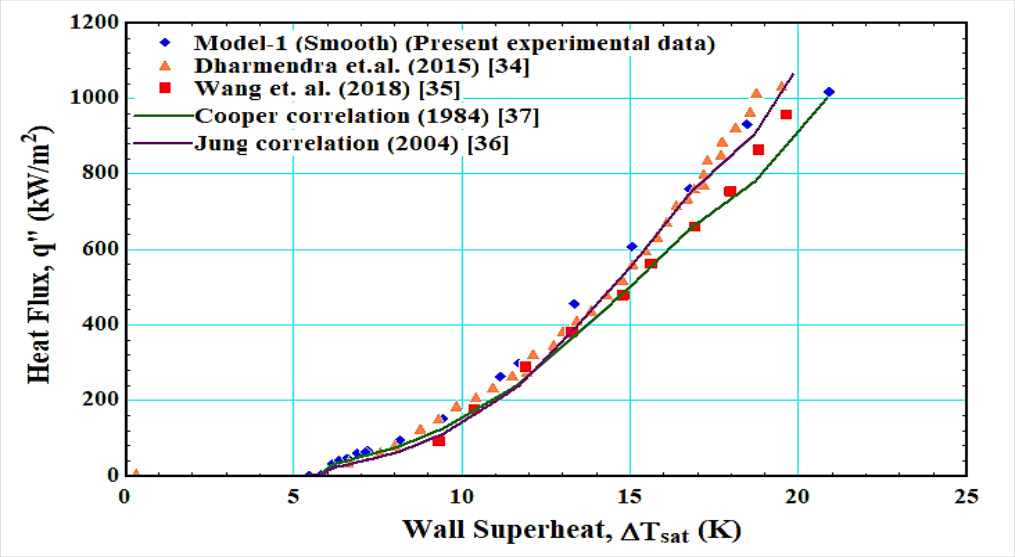

Figure 5: Comparison between present experimental data and previous work for smooth surface

4.2 Boiling curve

Figure 6 shows the boiling curves of Models 1 (smooth), 2 (CNT (1 g)), 3 (GNPs (1 g)) and 4 (CNT-GNPs (1:1) g). The smooth surface is used as a standard to figure out how much better nano-coating is. The graph shows that the wall is a little warmer than the distilled water's saturation temperature for a certain boiling curve and a low heat flux (q"). Because of this, the heat transfer in this area is completely due to the forced convection of single-phase liquid. As the applied heat flux increases, the wall superheat rises until it hits a critical point. At this point, even a small rise in q" causes the fluid to boil. This was clear from the graph, where the slopes of the lines changed sharply, showing the Onset of Nucleate Boiling (ONB). This means the change from a region with a single phase to a region with boiling has happened. When the ONB for coated surfaces is compared to the ONB for untreated surfaces, it is clear that the nanocoated surfaces need lower surface temperatures for ONB than the smooth surfaces. This could be because there were so many nucleation sites on the coated surfaces, which caused the nucleate boiling process to start very quickly, according to Gupta and Misra [4],[17]. For example, Model-1 (smooth surface), Model-2 (CNTs), and Model-3 (GNPs) all need 7.192 K, 4.634 K, and 4.012 K of wall superheat to start boiling. Based on these models, the heat flow needed to start boiling is 64.87, 156.3, and 30.03 kW/m^2, respectively. It is evident that the coated surface with GNPs has the lowest wall superheat and the lowest heat flux for the onset of nucleate boiling. Because of that, the boiling curve shifted to the left of the smooth surface. However, the responsible parameters for decreasing the wall superheat are the wettability and a roughness effect if the current surfaces' roughness served as nucleation cavities during boiling, as explained by Gupta and Misra [4],[17], and Kim et al. [35]. Kandlikar's theory [36] was used to determine the range of active nucleation cavities and guess the size of a cavity that could act as a nucleation seed using the expression of Equation 9 below:

$$r_{max}, r_{min} = \frac{\delta_{th}\sin\theta}{2.2}\cdot\frac{\Delta T_{sat}}{\Delta T_{sat}+\Delta T_{sub}}\left[1 \pm \sqrt{1 - 8.8\sigma T_{sat}\left(\frac{\Delta T_{sat}+\Delta T_{sub}}{\rho_v h_{fg}\delta_{th}(\Delta T_{sat})^2}\right)}\right] \quad (9)$$

After using the experimental data, the range of nucleation holes found is shown in Table 1. Based on this table, we can say that the surfaces studied for GNPs were rough enough that the hole sizes were within the expected range, and they were also very wet.

As shown in Figure 6, the coated surface has helped get a smaller wall superheat than the smooth surface under mild and high heat flux conditions. At the same wall superheat, the heat flow was much higher through the covered surfaces than through the smooth surfaces. In this case, at a wall superheat of 11 K, the heat flux was 180 kW/m^2 for the smooth surface and 800 kW/m^2 for the coated surfaces with CNTs and GNPs. Dong et al. [37] also found that nanostructures might improve the heat flux compared to smooth surfaces at the same wall superheat. This result is similar to theirs. Because of this, CHF increased by 42% and 102% on covered surfaces Models 2 (CNT) and 3 (GNPs) compared to smooth surfaces. Model 3 showed the biggest increase because it had more pores and was easier to wet. This is because the microlayer bubble covers a larger area of hydrophilic-coated surfaces. This makes the dry area smaller and improves the cooking process.

Figure 6 shows the boiling curve for Model-4, a nanocomposite-covered surface with CNT-GNPs (1:1) g. It also shows Models 1 (smooth), 2 (CNT (1 g)), and 3 (GNPs (1 g)) with nanoparticles on top to illustrate the extent of improvement.The ONB for Models 1, 2, 3, and 4 was about 7.192 K, 4.634 K, 4.012 K, and 3.93 K, respectively, as shown in this graph. This means that Model-4 has an ONB slightly lower than coated models. We can say that a nanocomposite-coated surface can lower the wall superheat needed to start heating. According to Dong et al. [37], higher roughness, seen in Table 1, caused the bubbles' contact diameter and exit diameter to get smaller. There are more nucleation sites in Model-4, which lowers the wall superheat. It is easy to see that the boiling curves of Model-4 and Model-3 overlap as the heat flux rises above the ONB. This happens until the heat flux reaches about 1100 kW/m^2. In this range, the heat transfer is not affected by the covering material, CNT. After that, Model-4's boiling curve moved to the right. This is thought to be because of the hydrophobic material (CNT) effect. Because of this, Model-4 improved CHF by about 68% compared to Model-1. This is more than Model 2 but less than Model 3.

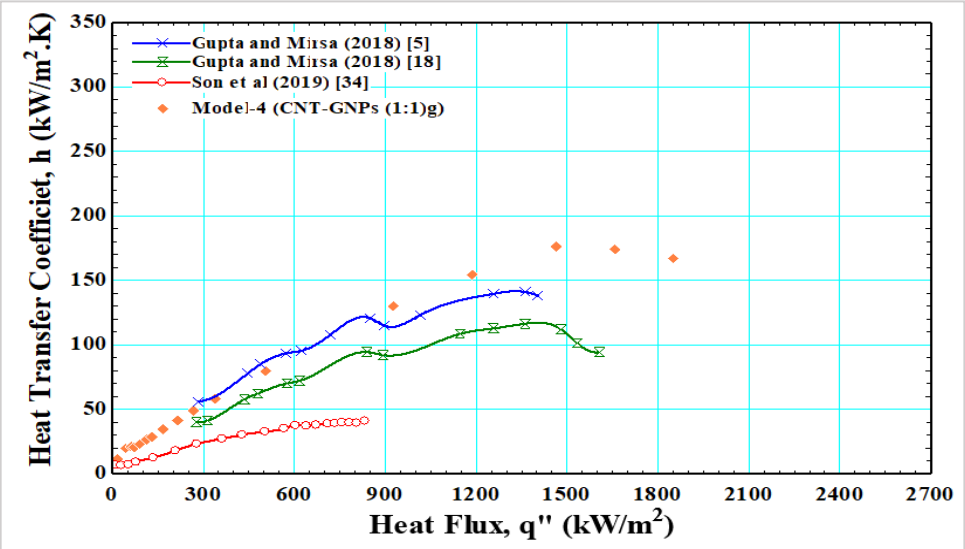

Figure 6: Effect of nano- and nanocomposite coating on boiling curve

4.3 Heat transfer coefficient

Figure 7 illustrates the influence of nanocoated surfaces on the heat transfer coefficient in relation to the heat flow for Models 1 (smooth surface), 2 (CNT (1 g)), 3 (GNPs (1 g)), 4 (CNT-GNPs (1:1) g). The figure illustrates that the heat transfer coefficient for all models exhibits a comparable trend to the heat flux. In general, the Figure illustrates that for every tested surface under low heat flux conditions, there is a distinct and abrupt rise in the heat transfer coefficient values during the initial boiling stage. Therefore, when the heat flux increases, the heat transfer coefficients will also grow until they reach their maximum value. However, after this point, the heat transfer coefficients experience a significant deterioration at higher heat flux levels. The phenomenon under consideration can be elucidated by the findings of Fan et al. [21], who observed a positive relation between the nucleation sites and the escalation of heat flux. Subsequently, with the escalation of heat flux and the proliferation of bubble nucleation sites, the proximity of bubbles leads to mutual interference and coalescence, giving rise to larger bubbles. Ultimately, this culminates in developing a vapor blanket on the surface undergoing boiling. In instances with significant heat flux, the presence of a vapor blanket can significantly impair heat transfer efficiency. This is due to the vapor blanket's ability to impede the departure of bubbles and the re-establishment of liquid contact with the boiling surface. This is supported by the HTC exhibiting a declining tendency, as depicted in the image.

Based on the data presented in the figure, it is apparent that the heat transfer coefficient (HTC) for Model 2 exceeds that of Models 1 and 3 when subjected to a heat flux below 300 kW/m^2. This discrepancy can be attributed to the hydrophobic surface characteristics of Model 2. Based on the observed rise in heat flux, it can be inferred that the heat transfer coefficient for Model 3 surpasses that of Models 2 and 1. In a broader context, the maximum heat transfer coefficients for Models 1, 2, and 3 were recorded as 49.2, 69, 110, and 217 kW/m^{2}K. Therefore, an increase in the HTC was observed for Models 2 and 3, compared to Model 1, which was 48% and 132%, respectively. The HTC value for Model-3 is observed to be the highest among the tested models, primarily attributed to its elevated roughness. The observed phenomenon can be attributed to the influence of surface roughness on the formation of nucleation cavities. This relationship is evident from the data presented in Table 1, which indicates that the estimated size of the cavities aligns with the surface under investigation. Consequently, cavities inside the porous structure will lead to an increased number of active nucleation sites.

Additionally, the surface covered with 1 gram of graphene nano-platelets (GNPs) in Model-3 exhibits reduced pore diameters. A reduced cavity radius corresponds to a diminished surface tension at the base of the vapor bubble, necessitating a decreased buoyancy force for the bubble's detachment. This phenomenon implies that more active nucleation sites are producing vapor bubbles, significantly augmenting the heat transfer coefficient (HTC).

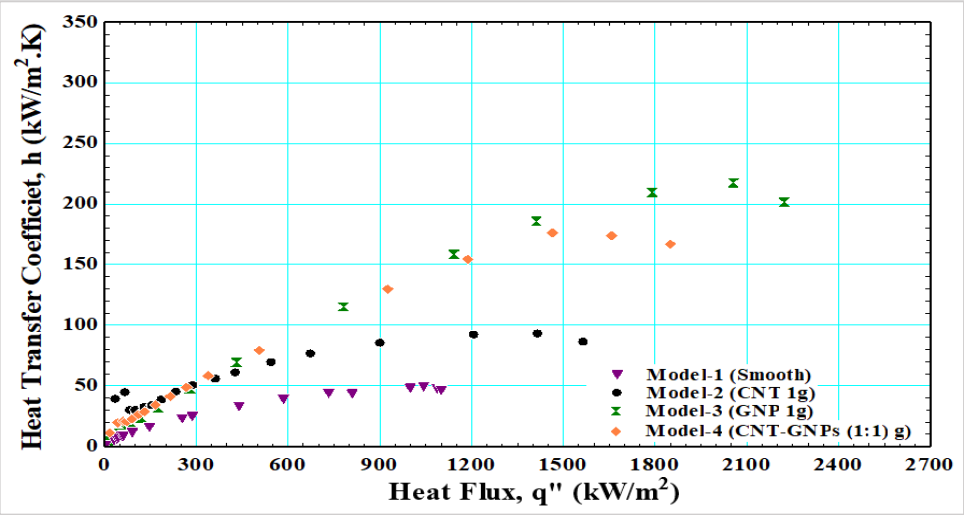

Figure 7: Effect of nano- and nanocomposite coating on heat transfer coefficient

Figure 7 depicts the relationship between the heat transfer coefficient and the heat flux for the nanocomposite coating on the copper surface, namely the CNT-GNPs (1:1) g (Model-4). In addition, the image presented in this study showcases the nanocoated surface Models 2 (CNT (1 g)) and 3 (GNPs (1 g)), alongside Model-1, to assess the improvement in heat transfer coefficient (HTC). The curve behavior exhibited by Model 4 is comparable to Models 1, 2, and 3. As depicted in the figure, when the heat flux is below 1300 kW/m^2, the heat transfer coefficients (HTC) for Model-3 and Model-4 exhibit significant overlap. This indicates that the coated surface possesses hydrophilic properties, specifically due to the presence of GNPs, and remains unaffected by the hydrophobic substance CNT. The impact of carbon nanotubes (CNT) was observed when the heat flow exceeded 1300 kW/m^2, decreasing the heat transfer coefficient. This coefficient was found to be lower than that of Model 3.

In contrast to Model 1, Models 2, 3, and 4 exhibited enhanced heat transfer coefficients of 48%, 132%, and 154%, respectively, within the identical heat flux range of 0-1100. The data presented in Table 1 demonstrates a clear relation between the maximum augmentation of Model-4 and its higher roughness.

4.4 Validation of the current results

4.4.1 Comparison with previous nanocoating works

The comparison of HTC for the present study of models 2 and 3 with performance available in previous works, such as Katarkar et al. [18], Moghadasi and Saffari [38], Xie et al. [39], and Godinez et al. [40] are presented in Figure 8. According to the figure, comparing Models 2 and 3 with the data for Katarkar et al. [21] revealed good predictions for Models 3, with an MAE of 19.6%. While it predicted underprediction for model-2 with an MAE of 81.1%, This could be returned as follows: Electro-deposition coating method with two steps, coating material (GNPs) with a concentration of 400 mg/l, and the working fluid (R-134a). The data for Moghadasi and Saffari [38] predicted very well for Model 2 with an MAE of 19.9%, while it was poorly predicted for Model 3 with an MAE of 31.2%. This is attributed to the coating method (spin coating) and coating material (Fe_3O_4). Godinez`s results predicted well with Models 2 and 3 with an MAE of 24.2% and 21.9%, respectively. Xie et al. [39] data showed a good prediction for Model 2 with an MAE of 20%, whereas there was a poor prediction for Model 3, with an MAE of 42.5%. This could be attributed to the chemical treatment coating method and the time consumed.

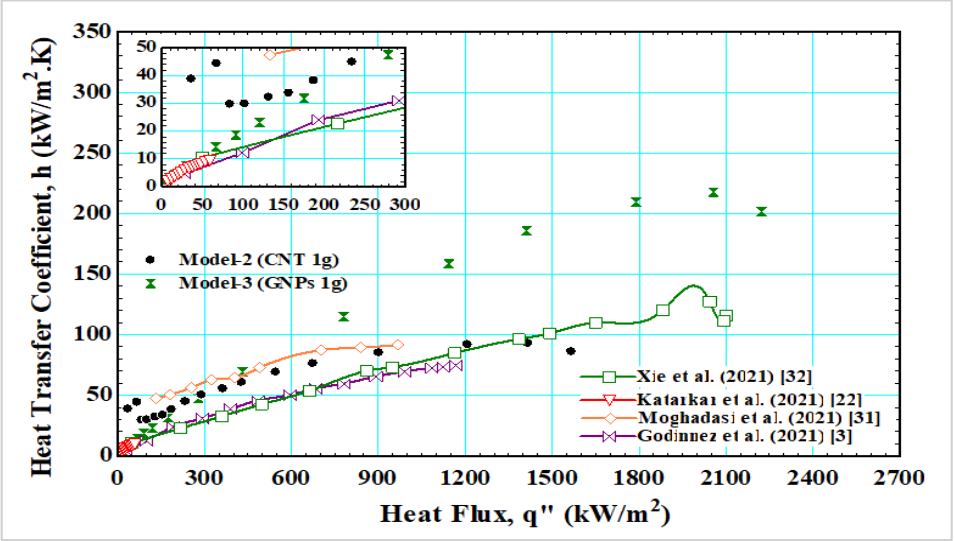

Figure 8: Comparison of nano-coating with previous works

4.4.2 Comparison with previous nanocomposite works

For the data of the HTC of the nanocomposite surface for the present work, Model-4 (CNT-GNPs (1:1) g) was compared with previous work like Gupta and Mirsa [4][17], and Son et al. [20], as shown in Figure 9. The comparison with Gupta and Mirsa [27] shows that it is very well predicted for Model-4 with an MAE of 9.14%. This is due to the use of a two-step electro-deposition coating method and the Cu-Al_2O_3 composite coating material. A good prediction was also found, with an MAE of 28.6%, compared with Gupta and Mirsa [4]. Referring to the figure, the data for Son et al. [20] predicted Model 4 with an MAE of 59.9%. This is because the deposition of FeCrAl by the direct current magnetron coating method on the heating surface has a cylindrical shape.

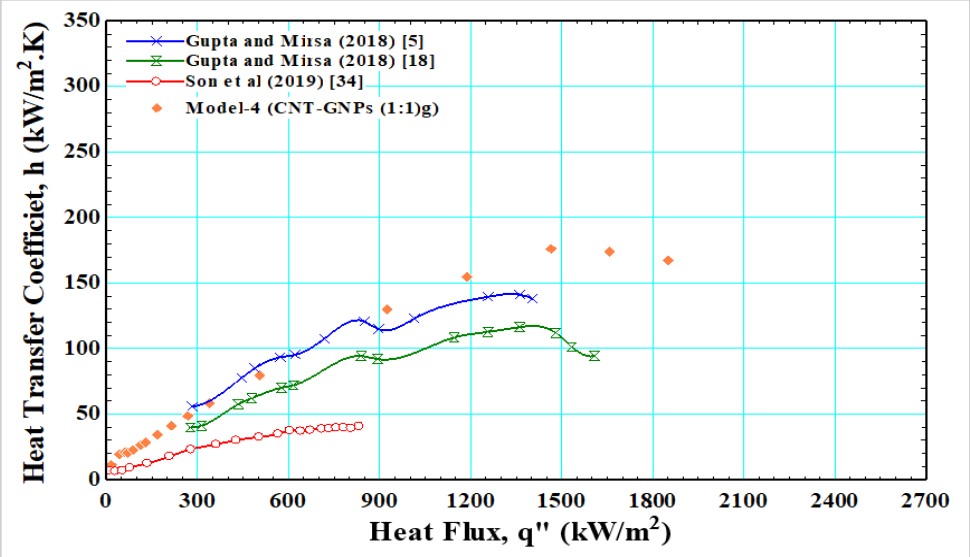

Figure 9: Comparison of nanocomposite coating with previous works

5. Conclusion

The experiments were conducted using deionized water at atmospheric pressure to examine the impact of coating characteristics on the boiling performance of three coating surface models with a constant coating thickness. Plane surfaces were utilized for comparison.

The empirical investigations examined in this chapter resulted in the subsequent findings:

1) The boiling performance of hydrophilic surfaces (Model-3) is greater than that of hydrophobic surfaces (Model-2). The CHF increases as the contact angle decreases, allowing more bubbles to depart.
2) The critical heat flux (CHF) point for the GNP surface is located at the top limit of the CHF range. The elevated value of CHF can be ascribed to the porosity of the GNPs coating, which facilitates wicking in combination with the presence of cavities within the coating. The wicking process facilitates the reintroduction of liquid into the porous coating, while cavities enhance the boiling curve and augment the nucleate boiling heat transfer coefficient.
3) The CNT-GNPs are a mixture of hydrophobic and hydrophilic materials that could provide a mixed effect of wettability.
4) When comparing mixed surfaces to pure hydrophilic surfaces, it is seen that the former exhibits a higher HTC than hydrophilic surfaces at low superheat degrees. However, the mixed surfaces demonstrated a larger CHF than hydrophobic surfaces at high superheat degrees. Hence, the mixed surfaces exhibited greater adaptability to a broader spectrum of applied heat flux.
5) The maximum enhancement in CHF is achieved by Model-3 with 102%, and the maximum enhancement in CHF is achieved by Model-4 with 154% when it is compared with the plain surface.

Author contributions

Conceptualization, A. Al-Obaidy, E. Fayyadh,. and A. Al-Dabagh; data curation, A. Al-Obaidy; investigation, A. Al-Obaidy, E. Fayyadh,. and A. Al-Dabagh.; methodology, A. Al-Obaidy.; project administration, E. Fayyadh,. and A. Al-Dabagh, resources, A. Al-Obaidy.; supervision, E. Fayyadh,. and A. Al-Dabagh; validation, A. Al-Obaidy, E. Fayyadh,. and A. Al-Dabagh; writing—original draft preparation, A. Al-Obaidy, E. Fayyadh,. and A. Al-Dabagh; writing—review and editing, A. Al-Obaidy, E. Fayyadh,. and A. Al-Dabagh All authors have read and agreed to the published version of the manuscript.

Funding

This research received no specific grant from any funding agency in the public, commercial, or not-for-profit sectors.

Data availability statement

The data that support the findings of this study are available on request from the corresponding author.

Conflicts of interest

The authors declare that there is no conflict of interest.

Nomenclatures

Symbol	Description	Symbol	Description
Latins' symbols		**Greek symbols**	
A	Area	δ	boundary layer thickness
CHF	Critical Heat Flux	θ	Contact angle
CNT	Carbon Nanotube	ρ	Density
EDM	Electrical Discharge Machine	σ	Surface tension
D	Diameter	**Subscripts**	
GNPs	Graphene Nanopletes	l	Liquid
HTC / h	Heat transfer coefficient	s	Surface
h_{fg}	Latent heat of vaporization	Sat	Saturated
I	Electrical current	Sub	Subcooled
k	Thermal conductivity	Th	Thermal
MAE	Mean absolute error	v	Vapor
q	Heat flux		
R	Roughness		
ONB	Onset of nucleate boiling		
r,min/r,max	Maximum and minimum cavity radius		
T	Temperature		
U	Uncertainty		
V	Voltage		
W	Width		
y	Distance between thermocouples		

References

[1] D. V. Kuznetsov, A. N. Pavlenko, A. A. Radyuk, D. I. Komlev, and V. I. Kalita, Features of Heat Transfer during Pool Boiling of Nitrogen on Surfaces with Capillary-Porous Coatings of Various Thicknesses, J. Eng. Thermophys., 29 (2020) 375–387. https://doi.org/10.1134/S1810232820030017

[2] H. S. Jo et al., Supersonically spray-coated copper meshes as textured surfaces for pool boiling, Int. J. Therm. Sci., 132 (2018) 26–33. https://doi.org/10.1016/j.ijthermalsci.2018.05.041

[3] J. M. Kim, B. T. Kong, H. B. R. Lee, S. Wongwises, and H. S. Ahn, Effect of h-BN coating on nucleate boiling heat transfer performance in pool boiling, Exp. Therm. Fluid Sci., 98 (2018) 12–19. https://doi.org/10.1016/j.expthermflusci.2018.05.010

[4] S. K. Gupta and R. D. Misra, Effect of two-step electrodeposited Cu–TiO_2 nanocomposite coating on pool boiling heat transfer performance, J. Therm. Anal. Calorim., 136 (2019) 1781–1793. https://doi.org/10.1007/s10973-018-7805-7

[5] Z. Cao, Z. Wu, S. Abbood, and B. Sundén, An analysis of pool boiling heat transfer on nanoparticle-coated surfaces, Energy Procedia, 158 (2019) 5880–5887. https://doi.org/10.1016/j.egypro.2019.01.537

[6] Q. A. Al-Nakeeb, E. M. Fayyadh , and M. R. Hasan, Experimental Investigation of Artificial Cavities Effect of Single-Phase Fluid Flow and Heat Transfer in Single Microchannel, Eng. Technol. J., 40 (2022) 109–119. http://doi.org/10.30684/etj.v40i1.2122

[7] Z. K. Kadhim, A. A. Mohamed, and S. A. Abed, An Experimental Study for the Effect of Vertical Forced Vibration on Pool Boiling Heat Transfer Coefficient, Eng. Technol. J., 30 (2012) 1662–1676. https://doi.org/10.30684/etj.30.10.1

[8] B. Ahmed Abid and M. Kamel Getan, Heat Transfer in Pool Boiling with Surfactants, Eng. Technol. J., 28 (2010). https://doi.org/10.30684/etj.28.17.3

[9] S. mohammed and E. Fayyadh, Experimental Investigation of Sub-Cooled Flow Boiling in Metallic Microchannel, Eng. Technol. J., 37 (2019) 408–415. https://doi.org/10.30684/etj.37.10a.5

[10] J. M.Ali, B. Ahmed Abid, and K. M. Essa, Pool Boiling Heat Transfer Using Nanofluids, Eng. Technol. J., 33 (1015) 512–525. https://doi.org/10.30684/etj.33.2a.5

[11] A. Ali et al., Ion irradiation effects on Cr-coated zircaloy-4 surface wettability and pool boiling critical heat flux, Nucl. Eng. Des., 362 (2020) 110581. https://doi.org/10.1016/j.nucengdes.2020.110581

[12] H. S. Ahn et al., Pool boiling CHF enhancement by micro/nanoscale modification of zircaloy-4 surface, in Nucl. Eng. Des., 240 (2010) 3350–3360. https://doi.org/10.1016/j.nucengdes.2010.07.006

[13] E. Forrest, E. Williamson, J. Buongiorno, L. W. Hu, M. Rubner, and R. Cohen, Augmentation of nucleate boiling heat transfer and critical heat flux using nanoparticle thin-film coatings, Int. J. Heat. Mass. Transf., 53 (2010) 58–67. https://doi.org/10.1016/j.ijheatmasstransfer.2009.10.008

[14] S. Abdul Jabbar, A. Jawad Sultan and H. Alaa Maabad, Prediction of Heat Transfer Coefficient of Pool Boiling Using Back propagation Neural Network, Eng. Technol. J., 30 (2012) 1293–1305. https://doi.org/10.30684/etj.30.8.1

[15] H. Chu, N. Xu, X. Yu, H. Jiang, W. Ma, and F. Qiao, Review of surface modification in pool boiling application: Coating manufacturing process and heat transfer enhancement mechanism, Appl. Therm. Eng., 215 (2022) 119041. https://doi.org/10.1016/j.applthermaleng.2022.119041

[16] C. M. Patil, K. S. V. Santhanam, and S. G. Kandlikar, Development of a two-step electro-deposition process for enhancing pool boiling, Int. J. Heat Mass Transf., 79 (2014) 989–1001. https://doi.org/10.1016/j.ijheatmasstransfer.2014.08.062

[17] S. K. Gupta and R. D. Misra, An experimental investigation on pool boiling heat transfer enhancement using Cu-Al_2O_3 nano-composite coating, Exp. Heat Transf., 32 (2019) 133–158. https://doi.org/10.1080/08916152.2018.1485785

[18] J. Li, W. Fu, B. Zhang, G. Zhu, and N. Miljkovic, Ultrascalable Three-Tier Hierarchical Nanoengineered Surfaces for Optimized Boiling, ACS Nano, 13 (2019) 14080–14093. https://doi.org/10.1021/acsnano.9b06501

[19] A. M. Rishi, S. G. Kandlikar, and A. Gupta, Improved wettability of graphene nano-platelets (GNP)/copper porous coatings for dramatic improvements in pool boiling heat transfer, Int. J. Heat Mass Transf., 132 (2019) 462–472. https://doi.org/10.1016/j.ijheatmasstransfer.2018.11.169

[20] D. C. Mo, S. Yang, J. L. Luo, Y. Q. Wang, and S. S. Lyu, Enhanced pool boiling performance of a porous honeycomb copper surface with radial diameter gradient, Int. J. Heat Mass Transf., 157 (2020) 119867. https://doi.org/10.1016/j.ijheatmasstransfer.2020.119867

[21] A. S. Katarkar, A. D. Pingale, S. U. Belgamwar, and S. Bhaumik, Effect of GNPs Concentration on the Pool Boiling Performance of R-134a on Cu-GNPs Nanocomposite Coatings Prepared by a Two-Step Electro-deposition Method, Int. J. Thermophys., 42 (2021). https://doi.org/10.1007/s10765-021-02876-z

[22] K. Yim, J. Lee, B. Naccarato, and K. J. Kim, Surface wettability effect on nucleate pool boiling heat transfer with titanium oxide (TiO_2) coated heating surface, Int. J. Heat Mass Transf., 133 (2019) 352–358. https://doi.org/10.1016/j.ijheatmasstransfer.2018.12.075

[23] H. H. Son, Y. S. Cho, and S. J. Kim, Experimental study of saturated pool boiling heat transfer with FeCrAl- and Cr-layered vertical tubes under atmospheric pressure, Int. J. Heat Mass Transf., 128 (2019) 418–430. https://doi.org/10.1016/j.ijheatmasstransfer.2018.09.013

[24] S. Fan, W. Tong, and F. Duan, Nucleate pool boiling heat transfer enhancement in saturated Novec 7100 using titanium dioxide nanotube arrays, Int. Commun. Heat Mass Transfer, 122 (2021) 105166. https://doi.org/10.1016/j.icheatmasstransfer.2021.105166

[25] B. Bourdon, P. Di Marco, R. Rioboo, M. Marengo, and J. De Coninck, Enhancing the onset of pool boiling by wettability modification on nanometrically smooth surfaces, Int. Commun. Heat Mass Transfer, 45 (2013) 11–15. https://doi.org/10.1016/j.icheatmasstransfer.2013.04.009

[26] D. Y. Lim and I. C. Bang, Controlled bubble departure diameter on biphilic surfaces for enhanced pool boiling heat transfer performance, Int. J. Heat Mass Transf., 150 (2020) 119360. https://doi.org/10.1016/j.ijheatmasstransfer.2020.119360

[27] Y. Li, Y. Li, W. Jiao, X. Chen, and G. Lu, Manipulating the heat transfer of pool boiling by tuning the bubble dynamics with mixed wettability surfaces, Int. J. Heat Mass Transf., 170 (2021) 120996. https://doi.org/10.1016/j.ijheatmasstransfer.2021.120996

[28] C. Park et al., Pool boiling enhancement using hierarchically structured ZnO nanowires grown via electrospraying and chemical bath deposition, Appl. Therm. Eng., 187 (2021) 116553. https://doi.org/10.1016/j.applthermaleng.2021.116553

[29] A. Mehdikhani, H. Moghadasi, and H. Saffari, An experimental investigation of pool boiling augmentation using four-step electrodeposited micro/nanostructured porous surface in distilled water, Int. J. Mech. Sci., 187 (2020) 105924. https://doi.org/10.1016/j.ijmecsci.2020.105924

[30] A. Kalani , S. G. Kandlikar, Pool Boiling Of Fc-87 Over Microchannel Surfaces At Atmospheric Pressure, Proceedings of the ASME 2012 International Mechanical Engineering Congress and Exposition, Houston, Texas, USA, 7, 2012, 2051-2057. https://doi.org/10.1115/IMECE2012-86186.

[31] A. Kalani , S. G. Kandlikar, Pool Boiling Heat Transfer Over Microchannel Surfaces With Ethanol At Atmospheric Pressure, ASME 2012 10th International Conference on Nanochannels, Microchannels, and Minichannels. Rio Grande, Puerto Rico, USA, 2012, 333-339. https://doi.org/10.1115/ICNMM2012-73188

[32] Coleman, H. W. and Steele, W. G. Experimentation, validation, and uncertainty analysis for engineers, John Wiley & Sons, 2018.

[33] M. Dharmendra, S. Suresh, C. S. Sujith Kumar, and Q. Yang, Pool boiling heat transfer enhancement using vertically aligned carbon nanotube coatings on a copper substrate, Appl. Therm. Eng., 99 (2016) 61–71. https://doi.org/10.1016/j.applthermaleng.2015.12.081

[34] Y. Q. Wang, J. L. Luo, Y. Heng, D. C. Mo, and S. S. Lyu, Wettability modification to further enhance the pool boiling performance of the micro nano bi-porous copper surface structure, Int. J. Heat Mass Transf., 119 (2018) 333–342. https://doi.org/10.1016/j.ijheatmasstransfer.2017.11.080

[35] D. Jung, H. Lee, D. Bae, and S. Oho, Nucleate boiling heat transfer coefficients of flammable refrigerants, Int. J. Refrig., 27 (2004) 409–414. https://doi.org/10.1016/j.ijrefrig.2003.11.007

[36] M. G. Cooper, Saturation nucleate pool boiling - A simple correlation, in Institution of Chemical Engineers Symposium Series, J. Inst. Eng. Chem., (1984) 785–793. https://doi.org/10.1016/b978-0-85295-175-0.50013-8

[37] J. M. Kim, D. I. Yu, H. S. Park, K. Moriyama, and M. H. Kim, Smart surface in pool boiling: Thermally-induced wetting transition, Int. J. Heat Mass Transf., 109 (2017) 231–241. https://doi.org/10.1016/j.ijheatmasstransfer.2017.02.009

[38] S. G. Kandlikar, High flux heat removal with microchannels - A roadmap of challenges and opportunities, Heat Transfer Eng., 26 (2005) 5–14. https://doi.org/10.1080/01457630591003655

[39] L. Dong, X. Quan, and P. Cheng, An experimental investigation of enhanced pool boiling heat transfer from surfaces with micro/nano-structures, Int. J. Heat Mass Transf., 71 (2014) 189–196. https://doi.org/10.1016/j.ijheatmasstransfer.2013.11.068

[40] H. Moghadasi and H. Saffari, Experimental study of nucleate pool boiling heat transfer improvement utilizing micro/nanoparticles porous coating on copper surfaces, Int. J. Mech. Sci., 196 (2021) 106270. https://doi.org/10.1016/j.ijmecsci.2021.106270

[41] S. Xie, M. Jiang, H. Kong, Q. Tong, and J. Zhao, An experimental investigation on the pool boiling of multi-orientated hierarchical structured surfaces, Int. J. Heat Mass Transf., 164 (2021) 120595. https://doi.org/10.1016/j.ijheatmasstransfer.2020.120595

[42] J. C. Godinez, H. Cho, D. Fadda, J. Lee, S. J. Park, and S. M. You, Effects of materials and microstructures on pool boiling of saturated water from metallic surfaces, Int. J. Therm. Sci., 165 (2021) 106929. https://doi.org/10.1016/j.ijthermalsci.2021.106929